Final Draft
of the original manuscript:

Ziehmer, M.; Tschoepe, A.; Birringer, R.; Markmann, J.:
Examination of the Energy Phase Space of Mixed Copper Grain Boundaries by Orientation Imaging Microscopy (OIM) and Sphere-on-a-Plate Method
In: Acta Materialia (2013) Elsevier

DOI: 10.1016/j.actamat.2013.05.042

Examination of the Energy Phase Space of Mixed Copper Grain Boundaries by EBSD and Sphere-on-a-Plate Method

Markus Ziehmer[a,1,*], Andreas Tschöpe[a], Rainer Birringer[a], Jürgen Markmann[b,c]

[a] *Universität des Saarlandes, FR 7.2 Experimentalphysik, 66041 Saarbrücken, Germany*
[b] *Helmholtz-Zentrum Geesthacht HZG, Institut für Werkstoffforschung, Werkstoffmechanik, 21502 Geesthacht, Germany*
[c] *Technische Universität Hamburg-Harburg, Institut für Werkstoffphysik und -technologie, 21073 Hamburg, Germany*

Abstract

This article reports about an experimental study of the energy phase space of mixed copper grain boundaries by a combination of electron backscatter diffraction (EBSD) and the so-called sphere-on-a-plate method. Single crystal copper spheres with diameters of few microns were sintered onto flat single crystal {111} copper plates, resulting in random initial grain boundary configurations. EBSD measurements together with an assumption about the grain boundary plane orientation were used for the determination of the five macroscopic degrees of freedom of the grain boundaries. The tilt and twist components of the grain boundaries were calculated making use of the Interface Plane Scheme representation of grain boundaries. Upon annealing, the spheres rotated along gradients in the grain boundary energy phase space. Thus, points of the trajectories of single spheres could be recorded between the single annealing steps, allowing for tracing the path of single spheres towards and into energy minima regions. The results gathered from 13 spheres underline a strong complexity of the grain boundary energy phase space.

*Corresponding author: markus.ziehmer@hzg.de
[1] Currently at: Helmholtz-Zentrum Geesthacht HZG, Institut für Werkstoffforschung, Werkstoffmechanik, 21502 Geesthacht, Germany

1. Introduction

The physical properties of polycrystalline materials are influenced to a large extent by their inherent defects [1]. One of these are the grain boundaries, which separate single crystalline regions of different orientation but same chemistry. The contribution of the grain boundaries to a material's properties stems from their volume fraction and their specific properties. It has been shown that extrema of grain boundary properties are often related to energy minima [2]. Thus, the grain boundary energy seems to be the decisive parameter, usually written as an excess Gibbs Free Energy term G^{gb}:

$$G^{\mathrm{gb}} = \gamma \cdot A, \tag{1}$$

where γ denotes the specific grain boundary energy, and A the grain boundary area.

Principally, γ depends on 8 degrees of freedom (DOF), necessary for a complete geometrical characterization of a grain boundary. Several descriptions of the five macroscopic DOF are possible, which emphasize different aspects [3]. The coincidence-site lattice (CSL) scheme focuses on the misorientation of the adjacent crystallites (3 DOF; one angle Θ_{mis} and one axis $\vec{r}_{\mathrm{mis}}$) while neglecting the orientation of the grain boundary plane (2 DOF; a normal unit vector $\vec{n}$ related to one of the grains) [4]. The inverse volume density of CSL sites is denoted by the parameter Σ. An alternative parameterization of the macroscopic DOF, the Interface Plane Scheme, highlights the importance of the grain boundary plane orientations in both crystals by assigning four DOF to the two grain boundary normal unit vectors $\vec{n}_{1,2}$ and one DOF to an angle ϕ_{twist} [3, 5] (see also Appendix A.2). The three microscopic DOF are referred to mutual translations of the two grains, forced by atomic relaxation processes during the equilibration of the grain boundary core region, and are of no further interest in what follows.

The consequently hyperdimensional grain boundary energy phase space might be summarized qualitatively in a simple picture as shown in Fig. 1.

Therein, the essential implications are: apart from the global energy minimum, the single crystalline state, there are a number of local energy minima located at special subsets of the 5 macroscopic DOF. The functional form of the minima regions is believed to be of cusp-like shape, i.e resembles a singularity, as a result of a dislocation model of grain boundaries.

In a seminal paper, Read and Shockley presented an energy calculation for small angle pure tilt grain boundaries that were modelled as infinite periodic lattice dislocation walls [6] . The energy was calculated from the long-range elastic strain fields taking account of the boundary plane orientation and assuming a constant dislocation core energy. It is solely the elastic energy part which is responsible for the cusp-like shape of the energy minimum regions through a $(-\Theta_{\mathrm{mis}} \ln \Theta_{\mathrm{mis}})$-dependency.

While the calculations had been done for the small angle region, Read and Shockley suggested that in the large angle region local energy minima exist with similar cusp-like behaviour for all configurations that cannot be built up by regularly spaced, periodic lattice dislocation arrangements. Such deviations were proposed and proven later to be accommodated by so-called secondary grain boundary dislocations [7, 8, 9]. Hence, similar to the small angle case, Read-Shockley types of local energy minima regions arise around special Σ-misorientations where the secondary dislocations accommodate the mismatch to the perfect CSL as the primary lattice dislocations do for the perfect crystal lattice.

The experimental determination of absolute or relative grain boundary energies for a series of pure tilt and twist boundaries with fixed low-index grain boundary planes in various fcc metals and other materials gave evidence of the existence of local energy minima for some special CSL-configurations, e.g. Σ3, 9, 11 for Cu [10, 11, 12, 13]. Due to the experimental approaches, these investigations automatically put the focus on the degrees of freedom related to the misorientations. However, the strong influence of grain boundary inclination on the energy of Σ3 boundaries in Cu was revealed by U. Wolf et al. [14]. D. Wolf performed extensive computer simulations on fcc Cu and Au

as well as bcc Fe and Mo, also investigating mixed boundaries with fixed tilt component and varying twist, further stressing a strong influence of the grain boundary plane orientations. [15]. Recently, new atomistic simulations have been performed to calculate grain boundary energies in fcc metals, and sampling a larger part of the phase space than was possible before [16]. In the last decade, automated methods have been developped to extract the five parameter grain boundary character distribution from 3D sampling using EBSD and serial sectioning methods and combine it with measurements of dihedral angles at triple junctions in order to determine relative grain boundary energies with respect to the five macroscopic DOF [17, 18]. The results from large numbers of grain boundaries again support the view that grain boundary energy anisotropy seems to be much stronger influenced by variations in the grain boundary plane orientation than by variations in the lattice misorientation, for an overview, see [19]. Also, high energy x-ray diffraction microscopy has been used recently for a non-destructive 3D microstructure reconstruction that can be used to extract five parameter grain boundary character distributions [20].

Unlike the aforementioned approaches, the so-called sphere-on-a-plate method dispenses with an explicit energy determination. This method comprises thermally induced free rotations of single crystalline spheres that are sintered onto flat single crystal substrates to form flat grain boundaries between sphere and plate. The rotations are driven by grain boundary energy gradients, directing the spheres into energy minima positions in phase space (for details see section 3). The evolution of single grain boundaries happen without constraints imposed by a microstructural grain boundary network and can be traced, principally. Originally proposed by Shewmon [21], the group of Gleiter applied the sphere-on-a-plate technique by firstly performing XRD texture measurements on large Cu and Ag sphere ensembles with random initial misorientations between spheres and substrate, e.g. [22, 23, 24]. The analysis of the final misorientations revealed the existence of many CSL-related local energy minima using low-index substrate (grain boundary) orientations. Erb investigated the temperature dependency of the Cu grain boundary energy

revealing that with increasing temperature a decreasing number of energy minima has been observed [25]. The method was expanded by several authors to detect and analyze single sphere rotations using different methods with several restrictions. Kuhn recorded the temporal evolution of the misorientations of two 200 μm large Cu spheres again using XRD texture measurements, where the final position of one sphere did not coincide with a high-angle CSL-orientation [26]. Mykura examined the trajectories of 22 large Cu spheres into CSL-minima with electron channeling patterns in the SEM [27], describing the rotations by using an inadequate cartesian coordinate system. Chan and Balluffi performed a high-resolution TEM analyis of the rotations of nanosized Au particles sintered onto a thin film at preselected pure tilt, pure twist and mixed initial misorientations near special CSL-orientations [28, 29]. The trajectories of the spheres were recorded by analyzing the dislocation arrangements, thus delivering an until then experimentally unrivaled representation of grain boundary energy phase space sections.

The rather young Electron Backscatter Diffraction (EBSD) based Orientation Imaging Microscopy (OIM)® method in a SEM in combination with sphere-on-a-plate samples allows for overcoming at least some of the disadvantages of the formerly applied approaches. In particular, the convenient extraction and evaluation of orientation data offers a strongly simplified analysis of sphere rotations through energy phase space. Furthermore, by using some of the calculations provided by Wolf and Lutsko in establishing their Interface Plane Scheme [5], EBSD orientation data can be used to split the grain boundary configurations into their tilt and twist components, finally representing several discrete configurations with the complete set of the 5 macroscopic DOF.

The present article reports of an examination of the energy phase space of mixed copper grain boundaries by the sphere-on-a-plate method and EBSD. Cu spheres were produced by a combined evaporation-dewetting technique, had diameters between 2 and 5 μm, and were sintered onto single crystalline Cu {111} oriented substrates (see sec. 2). Section 3 describes the experimental technique in more detail. The results gathered from 13 rotated spheres are represented

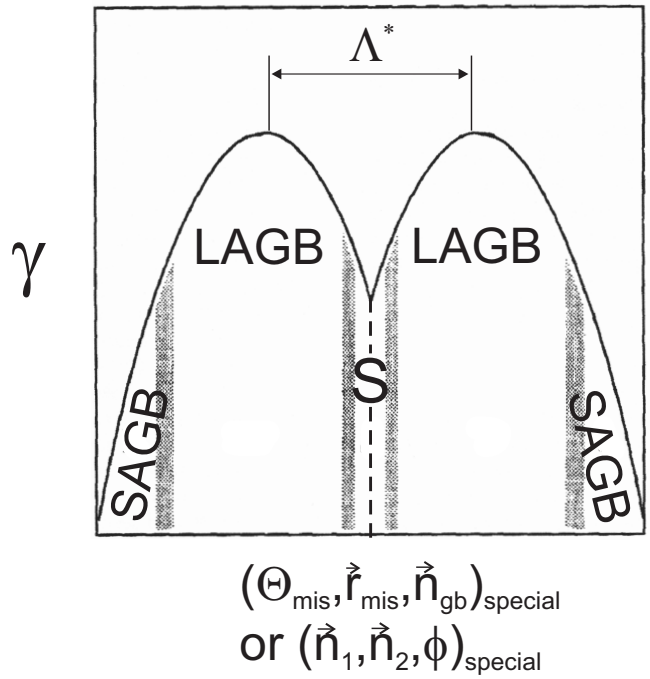

Figure 1: Sketch of the present view of grain boundary energy phase. Basically, it is divided into three regions SAGB (small angle grain boundaries), LAGB (large angle grain boundaries) and S (special low energy regions around special subsets of the macroscopic DOF, indicated by the dashed line) [2]. Λ^* denotes the catchment area of an energy minimum, where driving forces for sphere rotations are given.

and discussed in section 4 followed by a final summary. The appendix at the end of the paper provides basic mathematics with respect to data analysis.

2. Experimental

The single crystalline substrates had to fulfill several requirements. To avoid larger errors in the determination of the surface orientation of the plates, it was indispensable to provide surfaces as plane-parallel and smooth as possible. Furthermore, the samples had to be suitable for EBSD measurements, i.e. providing undeformed surfaces, which had been necessary as well to prevent recrystallization effects during the annealing steps. Therefore, high purity copper single crystalline {111} plates (3° max. deviation) cut from a single crystal grown by a Crzochalski method, with 20-25 mm in diameter and 2-3 mm thick, were pre-

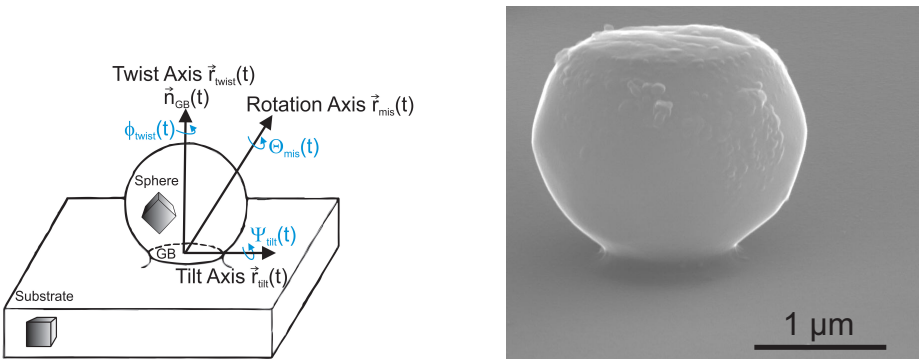

Figure 2: Sketch of the geometry of a sphere-on-a-plate sample (left) [30] and a SEM micrograph of a corresponding part of a Cu sample (right). Details of the synthesis are given in the text. The macroscopic DOF of the grain boundary at a certain time t are represented here in the CSL-notation by an angle Θ_{mis}, a rotation axis unit vector $\vec{r}_{\mathrm{mis}}$, and a grain boundary normal unit vector $\vec{n}$. Principally, this state can be split into the tilt and twist components $\Psi_{\mathrm{tilt}}, \vec{r}_{\mathrm{tilt}}$ and $\phi_{\mathrm{twist}}, \vec{r}_{\mathrm{twist}}$. Upon further annealing, the system can change its grain boundary state by unconstrained sphere rotations around any axis in order to decrease its grain boundary excess energy, thereby following energy gradients in phase space.

pared carefully by a sequence of standard mechanical and electrochemical metallographic surface treatment procedures. The substrates were cold mounted, SiC-paper grinded with grids not coarser than 1200 and subsequently diamond polished with particle sizes ranging from 15 μm down to 1 μm. The inevitably existent surface layer deformations which are always caused by the mechanical preparation methods were then removed by an electrochemical procedure, retaining the previously achieved smoothness of the surfaces. This last step involved the substrate operating as the anode and a large copper sheet operating as the cathode in a solution consisting of two volume shares methanol and one volume share nitric acid (65%). The solution was cooled down to 223-233 K and stirred slowly. The distance between the electrodes was roughly 50 mm. A DC voltage of 10-20 V was applied as long as necessary to remove the remaining scratches caused by the diamond polishing steps.

The single crystalline copper spheres were produced by a combined evaporation-dewetting method. High purity copper was evaporated onto a thin mica substrate, thus forming a film of desired thickness, which finally determined the size distribution of the copper spheres, resulting from a subse-

quent dewetting step. During this, the mica-copper sample was annealed in a furnace above the melting point of copper, kept there for 10 minutes in order to drive the dewetting of the melted copper and then slowly cooled down below the melting temperature. This procedure, performed in a reducing atmosphere ($95\%N_2, 5\%H_2$), led to the formation of small mostly single crystalline copper spheres (as confirmed by EBSD as far as possible), still fixed at the mica substrate.

Finally, the mica-copper sample was put upside down onto the copper single crystal plate, loaded with a small alumina piece, and annealed to start the sintering of the spheres on the copper substrate. Sintering parameters were different for different samples and are given explicitly in the following paragraphs. The whole sample synthesis procedures resulted in the formation of larger fields of similar sized spheres sintered onto the single crystalline substrate. In order to be able to identify single spheres from measurement to measurement, at first, it was necessary to find the fields in the SEM when remounting the sample after the annealing which took place in a furnace outside the SEM. Therefore, samples as well as microscope mounts were marked, and the microscope coordinates of such a field were recorded. Then, micrographs of a chosen field were taken and printed, and finally the spheres to measure were numbered consecutively.

The right side of Figure 2 shows a SEM micrograph of a sintered sphere on a copper substrate. The top of all spheres were flattened due to the inherent incomplete dewetting on the mica substrate. This turned out to be an advantage for EBSD measurements. The measurements of a large number of spheres indicated that the starting misorientations of the sintered spheres achieved by this sample synthesis procedure were randomly distributed.Although mica relics can be seen near the sphere's top, i.e. near the original mica substrate surface, facetting of the sphere surface in the lower half, i.e. around the grain boundary region, can be seen. This indicates to our belief that contamination in the grain boundary may be neglected, which otherwise might have lead to kinetic hindrances. A detailed discussion of potential kinetic barriers induced by impurities is given in section 4. Finally, at higher temperatures we noticed extensive

grain boundary migration crossing the entire spheres.

3. Method

Figure 2 clarifies the geometry and the principle of the sphere-on-a-plate method. Single crystalline spheres are sintered onto a single crystalline flat substrate. A grain boundary develops in the narrowest part of the sintering neck between sphere and substrate. Upon further annealing to overcome kinetic barriers, the sphere can rotate around any axis to reduce the grain boundary energy. Models describing rotation mechanisms and analyzing rotation rates can be found in [21, 29, 31, 32, 33]. Experimentally, the TEM-analysis by Chan and Balluffi proved the mechanisms to be simultaneous glide and climb of screw and edge dislocations [28, 29].

EBSD in SEM allows for automatic determination of the orientations of the spheres and the substrate in laboratory coordinates from which the misorientations could be calculated. Additionally, assuming the grain boundary plane normal to be perpendicular to the substrate surface and parallel to the EBSD normal direction a splitting of the single misorientation states of the sphere-substrate bicrystals into their corresponding tilt and twist components Ψ_{tilt} and ϕ_{twist} could be carried out by the aid of the Interface Plane Scheme, introduced by Wolf and Lutsko [5]. Thus, a more detailed view of the trajectories through orientation phase space was possible by detecting and recording the misorientation of single spheres at different times t between the single annealing steps. Figure 3 gives an example of the time-dependent evolution of the misorientation angle Θ_{mis} and the corresponding tilt and twist components Ψ_{tilt} and ϕ_{twist} for two undoubtedly rotated spheres. Time zero indicates the initial state after sintering. The samples were annealed outside the microscope in a reducing atmosphere. We visually confirmed the reduction of copper oxide layers even at temperatures as low as 623 K. Samples were stored in an inert gas glove box.

The EBSD measurements were performed by scanning across the upper flat parts of the truncated spheres (see Fig. 2) and the substrate beside the spheres. The arithmetic means of the six Euler-angles were determined and used to

calculate the two mean orientation matrices. Taking into account the 24 cubic symmetry operators, the 576 equivalent mean misorientations related to one grain were determined. The smallest misorientation angle, sometimes called disorientation angle, and the (24fold permuted) rotation axis were used as the final misorientation. The computed normalized surface orientation related to both substrate and sphere were used as the grain boundary plane normals $\vec{n_1}$ and $\vec{n_2}$, assuming both parallelism of substrate surface and grain boundary and parallelism of substrate surface normal and OIM z-axis. These grain boundary plane normals were used subsequently to calculate Ψ_{tilt} and ϕ_{twist} (see Appendix A.2). In order to get estimates of the measurement errors we performed a series of 16 measurements at one chosen sphere-substrate pair. Between the single measurements we removed the sample completely from the microscope as well as from the sample holder. This procedure enabled us to analyze the influence of non-perfect sample adjustment with respect to OIM coordinate systems, i.e. a tilt of the sample surface normal with respect to OIM z-axis. Note that different adjustments lead to different orientation matrices. This won‘t influence the misorientation values, but will effect the tilt and twist components, because of the different grain boundary normals calculated. On the basis of these measurements we decided to use the scatter of the respective measurements to indicate the error interval, i.e. Θ_{mis} (Ψ_{tilt}, ϕ_{twist}) is considered to be changed, if there is a clear tendency observable and a change between start value and final value of $\Delta\Theta_{\text{mis}}(\Delta\Psi_{\text{tilt}}, \Delta\phi_{\text{twist}}) \geq 0.5°(2.0°, 1.5°)$. Additionally, it was checked in how far a possible grain boundary plane tilting out of the surface orientation during annealing would have changed the tilt and twist components. Assuming grain boundary plane tilts of the order of the misorientation angle changes, maximum Ψ_{tilt} and ϕ_{twist} deviations of 0.5° and 0.1° were determined which do not change the conclusions derived from our examination. A detailed discussion of measurements and error analysis can be found in chapter 6 of [34].

Imaging and EBSD measurements were performed in a JEOL-7000F SEM equipped with an EDAX-TSL Digiview 3 Detector EBSD system with a high voltage of 25 kV at a working distance of 15 mm using a beam current of about

0.2 nA and a 2×2 pattern binning.

4. Results and Discussion

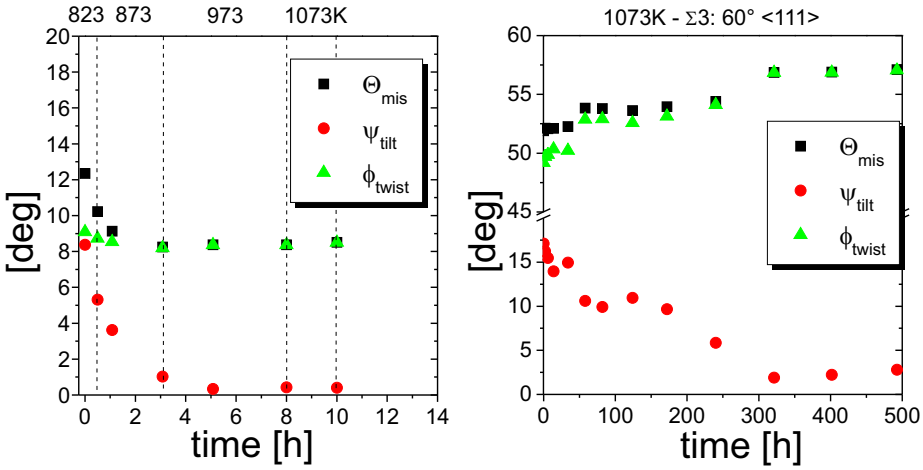

Figure 3: Exemplary graphs showing the temporal evolutions of misorientation angle Θ_{mis}, tilt angle Ψ_{tilt} and twist angle ϕ_{twist} of two spheres rotating towards two well-known energy minima. On the left, the non-isothermally induced rotation of one sphere towards coincidence is represented. A pure and possibly complete tilt reduction lead to the Θ_{mis}-changes as shown. Right-hand graph illustrates an isothermal sphere rotation towards the $\Sigma 3$ twin configuration effectuated by simultaneous tilt and twist angle changes. Both spheres missed the exact low-energy CSL-configurations clearly.

Due to the multidimensionality of the phase space a simple and comprehensive illustration of the results is difficult. In the following, the representations are chosen related to the specific aspects discussed. For details and all calculated graphs, see [34]. Only data of spheres with clearly resolved rotations are shown.

As explained in the introduction, sphere rotation is not possible until there are energy gradients $\partial\gamma/\partial\Theta$ in phase space building up a torque that acts on a sphere (Θ being representative for the five DOF). Once a sphere is localised within the catchment area Λ^* of an energy minimum (see Fig. 1) it will start rotating towards the special grain boundary configuration (which might comprise a CSL -related Σ misorientation) as long as the rotation mobility and the driving forces are sufficiently large.

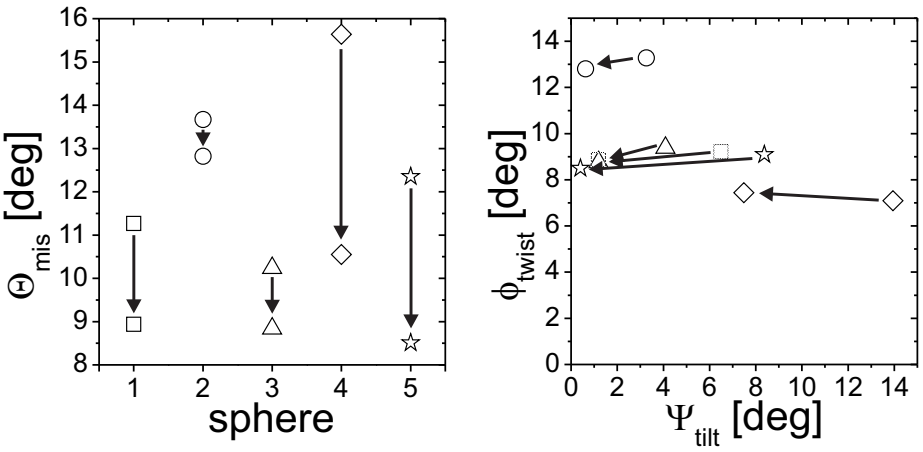

Figure 4: Summary of the developments of misorientation angles as well as the corresponding twist and tilt angles of five spheres rotating in the direction of the Σ1 coincidence indicated by the arrows in left-hand graph. The spheres were sintered at 873 K for 30 min and the annealing steps were: 0.5 h at 823 K, 2.5 h at 873 K, 5 h at 973 K, 2 h at 1073 K, and additional 3 h at 1173 K for spheres 2 and 3. Shown are the initial and final angles. Different rotation lengths as well as a lowest reached Θ_{mis}-limit of about 8.5° can be seen. Right-hand graph illustrates all rotations having been of pure tilt character, sometimes possibly leading to pure twist grain boundaries that were not decomposed upon further annealing.

Exemplarily, Figure 3 represents two such sphere rotations towards two well-known energy minima in terms of the temporal evolution of the misorientation angle Θ_{mis} and the respective tilt and twist angles Ψ_{tilt} and ϕ_{twist}. In one case the sphere rotation was generated by a non-isothermal annealing series as indicated in the graph with the sphere rotating towards the Σ1 coincidence configuration. The second graph displays the isothermally induced rotation of a sphere from a second sample in the direction of the Σ3: 60° <111> twin configuration (for annealing parameters see graphs). Clearly and surprisingly, both spheres missed the exact energy minimum configurations by far with rotation of the Σ1-sphere having stopped at about 8.5° and Σ3-sphere at 57.5°. The rotation towards Σ3 exhibited simultaneous tilt and twist changes with a final mixed grain boundary configuration after very long annealings at 1073K. In contrast, the rotation towards coincidence was accomplished by pure tilt changes, reducing Θ_{mis} from 12.5° to 8.5° and eliminating Ψ_{tilt} completely within the error margins (see sec. 3). No twist changes could be detected though, even in

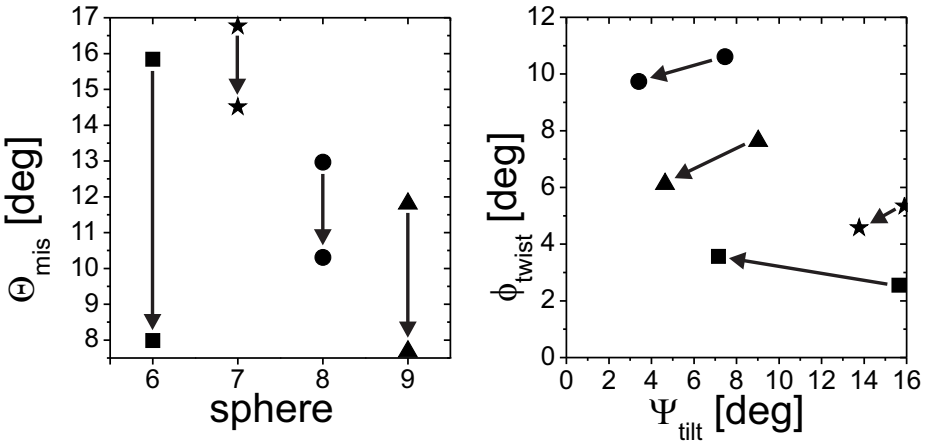

Figure 5: Summary of the developments of misorientation angles as well as the corresponding twist and tilt angles of another four spheres from a second sample rotating in the direction of the Σ1 coincidence indicated by the arrows in left-hand graph. In this case, the spheres were sintered at 623 K for 0.5 h and the annealing steps were: 1.3 h at 623 K ,22.25 h at 873 K, 14.5 h at 973 K, and 14.7 h at 1073 K. Shown are the initial and final angles. Again, different rotation lengths and a lowest reached Θ_{mis}-limit of about 7.5° can be seen. Right-hand graph demonstrates the rotations presumably having been of pure tilt character. Twist changes could not be resolved within the error margin. Complete tilt decompositions were not detected for these spheres

the case of annealing the assumably pure twist boundary at a temperature of 1073K. Relaxation of the tilt component implies that the energy gradient as well as the kinetic mobility are sufficient to allow a relaxation of the associated DOF. At the same temperatures, a reduction of the twist component was obviously prevented either by low driving force or reduced mobility, e.g. due to impurities. The use of mica substrate to prepare and sinter the spheres onto the single crystalline Cu plate provokes to look into alkali or silicate contamination at the boundaries. Local chemical analysis across the grain boundary core region and perpendicular to it using e.g. STEM in conjunction with EELS was beyond the scope of this study. However, based on the results presented in Fig. 3, the following rationale in favour of negligible contaminant induced barriers can be offered. Assuming for the sake of argument that impurities, originating from preparation and processing of the specimens, diffuse to the grain boundary core region to segregate or even form precipitates there. Small angle tilt and twist boundaries consist of arrays of edge and screw dislocations, respectively. While

the former are known to interact with contaminants by elastic strain effects leading to reduced mobility, this effect is much lower for screw dislocations because their stress field does not contain hydrostatic components. Therefore, we expect that glide of screw dislocations, which is responsible for the evolution of the twist angle, should be much less hampered by possible impurity interaction compared to climb of edge dislocations accompanying changes of the tilt angle. Coming back to Fig. 3 now, it is clearly revealed that the tilt decomposition during sphere rotation evolves within a few hours into coincidence, whereas, the twist decomposition is more or less stagnant. Overall, we believe that this observation rules out that impurity effects control the rotation kinetics. Instead, we are led to conclude that the rotation kinetic in fact probes the energy landscape.

There were 13 sphere rotations in total from different samples towards Σ-related configurations: $\Sigma 1$ (nine spheres), $\Sigma 3$ (two spheres), $\Sigma 9$ (one sphere) and $\Sigma 49b$ (one sphere). None of the $\Sigma 1$-rotations showed clear twist changes at temperatures up to 1073K, whereas all other rotations reduced their tilt and twist parts simultaneously (relating to the respective configurations). The exact CSL-configurations were never reached, even within 500h long-time annealings at 1073K.

Figure 4 and 5 summarize the results obtained from the nine spheres rotating towards the coincidence state by showing the initial and final misorientation, tilt and twist angles. In an attempt to exclude having lost twist changes during the sintering process, parameters were changed to lower temperatures and shorter times for one sample which lead to considerably smaller inital sintering necks, i.e. grain boundary diameters (see caption of Fig. 5 for detailed sintering and annealing parameters).

Although the nine spheres started at misorientation angles below 17° none of them reached the single crystalline state even approximately, with the lowest limit being about 8°. Rotation lenghts were different, no twist changes could be resolved within the error margins. Some of the spheres seem to have completely decomposed their tilt components, reaching a pure twist boundary state that surprisingly was maintained upon further annealing. In contrast some spheres

finalized in a mixed grain boundary state. Apparently, no simple rule exists to predict final sphere orientation states based on the initial states, reflecting the complexity of the hyperdimensional phase space. It seems as if the spheres had never reached the true small angle grain boundary catchment area. This might imply the existence of non-CSL energy minima since the final states could not be assigned to reasonable Σ-values or the existence of saddles in phase space where $d\gamma/d\Theta_{\mathrm{mis}} \approx 0$. Depending on the spheres‘ paths through phase space different final states were reached with different final deviations from the coincidence state.

Figures 6 and 7 show the evolutions of the respective rotation axes states and grain boundary orientation states. It can be seen that the nine spheres rotated along varying paths in phase space.

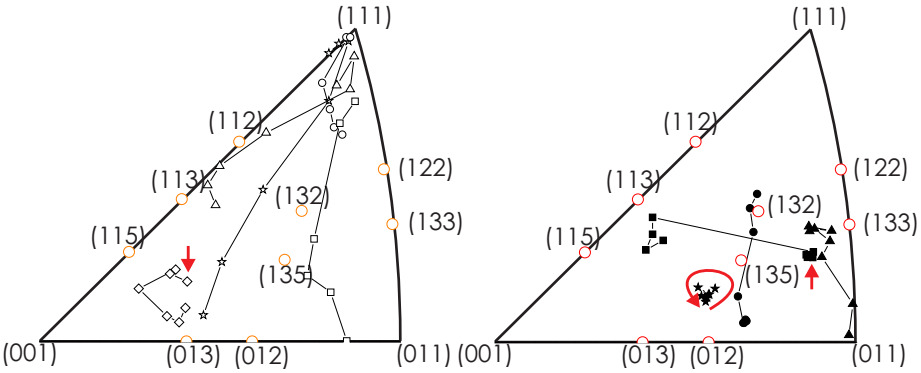

Figure 6: Inverse pole figures showing the evolutions of the respective misorientation rotation axes states $\vec{r}_{\mathrm{mis}}$ of sphere rotations from Fig. 4 (left-hand inverse pole figure) and 5 (right-hand inverse pole figure). Evolutions either proceeded towards the (111) direction or the final states are denoted by red arrows. From the pole figures it might be recognized that sphere rotations went on in different parts of orientation phase space.

Now, we consider sphere rotations with final grain boundary misorientation states near well-known large angle CSL energy minima. As described above, deviations from these special low energy configurations are accommodated structurally by secondary grain boundary dislocation networks, and their contribution to the grain boundary energy is treated analogous to the Read-Shockley analysis used for the small angle case. There were four spheres rotating to-

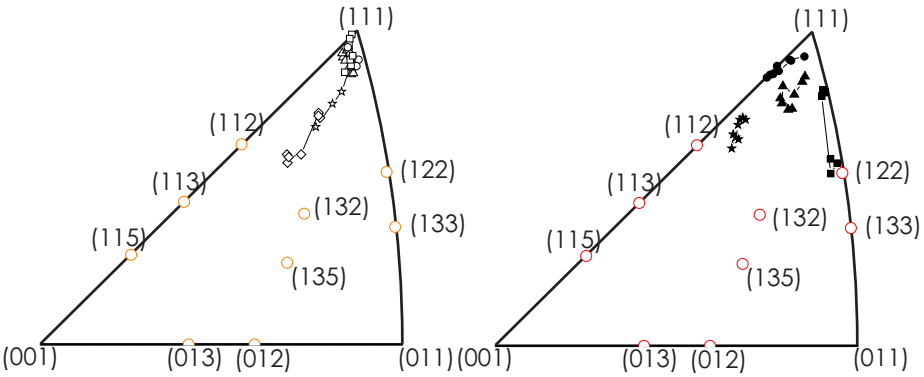

Figure 7: Inverse pole figures showing the evolutions of the respective grain boundaries plane orientation states $\vec{n}_{sphere}$ of sphere rotations from Fig. 4 (left-hand inverse pole figure) and 5 (right-hand inverse pole figure). Evolutions always proceeded towards the (111) direction. From the pole figures it might be recognized that sphere rotations went on in different parts of orientation phase space.

wards $\Sigma 3$ (one sphere with the same non-isothermal annealing treatment as the spheres shown in Fig. 5, see caption; one sphere isothermally, see Fig. 3, right graph), $\Sigma 9$ (isothermally as in Fig. 3, right graph), and $\Sigma 49b$ (isothermally as in Fig. 3, right graph). As already mentioned above, simultaneous tilt and twist changes were detected in all cases in contrast to the $\Sigma 1$-spheres. From Figure 8 the final angular deviations of the misorientation axes and angles from the exact high-angle Σ-states can be deduced. Although having approached the minima configurations much closer than the spheres in the $\Sigma 1$-case this might simply be attributed to reduced catchment areas. As in the small-angle case the existence of further minima near CSL-related or saddles might be indicated from our results.

A last annealing step of the non-isothermally annealed samples at 1173K lead to extensive grain boundary migration through the spheres, which also might again underline our belief that we do not have to consider kinetic problems resulting from contamination. From the SEM micrographs it was sometimes observed that the sintering necks evolved to a size larger than or comparable to sphere diameters, promoting grain boundary migration. On the other hand one sphere with a still smaller sintering neck that did not rotate at lower tempera-

tures might have *rotated* very close to the Σ1 configuration with

$$(\Theta_{mis}, \Psi_{tilt}, \phi_{twist})^{T\leq 1073K} = (15.0°, 5.1°, 14.1°),$$
$$(\Theta_{mis}, \Psi_{tilt}, \phi_{twist})^{T=1173K} = (0.9°, 0.6°, 0.7°).$$

Additionally, a sphere close to Σ21: 21.5°<111> switched to the exact CSL-configuration within the errors of measurement with

$$(\Theta_{mis}, \Psi_{tilt}, \phi_{twist})^{T\leq 1073K} = (23.6°, 5.4°, 23.0°),$$
$$(\Theta_{mis}, \Psi_{tilt}, \phi_{twist})^{T=1173K} = (21.7°, 0.3°, 21.7°),$$

thereby reducing the deviation of the rotation axis from the <111>-direction from 11.91° to 0.14°. Mykura observed Cu sphere rotations into Σ1 at temperatures of 1313K, i.e. close to the melting temperature [27]. It is well-known that the grain boundary energy has a temperature dependency via entropic contributions. Erb et al. showed that with increasing T the number of energy cusps reduces which in our case might lead to renewed rotations at 1173K of before locked spheres [25]. An orientation dependency of the entropy would lead to the observed manifold final sphere positions at 1073K compared to examinations performed at higher temperatures.

Interestingly, the isothermal annealing runs ending in near Σ3 and Σ9 states respectively showed a remarkable phenomenon in that the spheres reached and kept temporarily, i.e. over several annealing steps, Σ31*b* and 27a misorientation configurations very precisely with calculated misorientation rotation axis and angle deviations

$$dev(\vec{r}_{\mathrm{mis}}, \Theta_{mis})^{\Sigma 31b} < (0.1°, 0.5°),$$
$$dev(\vec{r}_{\mathrm{mis}}, \Theta_{mis})^{\Sigma 27a} < (0.5°, 0.1°).$$

These were left eventually upon ongoing annealing. Chan and Balluffi reported about what they called "'non-trapping cusps"' [28, 29]. Wolf concluded from these findings that grain boundary dislocations may be necessary to structurally accomodate misorientation, but that their energetic contribution may be

negligible because a rotation into a minima configuration followed by a rotation out of it would require the removal of grain boundary dislocations followed by a reintroduction of them [15].

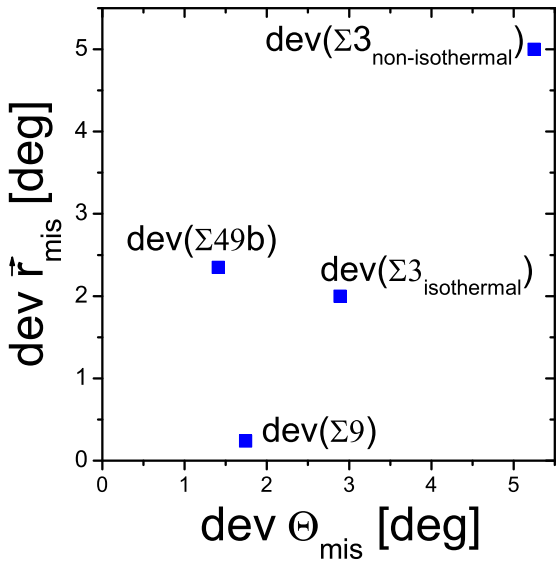

Figure 8: Representation of the final angular misorientation deviations from exact CSL-misorientations of four spheres having rotated towards Σ3, 9 and 49b as indicated.

5. Summary

We used the well-established sphere-on-a-plate method in combination with EBSD for an investigation of the multidimensional grain boundary energy phase space of Cu. This experimental approach dispenses with an explicit determination of relative or absolute energies. Instead, the gradients in grain boundary energy phase space are used to initiate the rotation of spheres sintered onto a flat substrate along these gradients. EBSD was used to analyze single points of the trajectories of single spheres from which conclusions could be drawn regarding the dependency of the specific grain boundary energy γ with respect to the five macroscopic DOF of a grain boundary. In total, the rotations of 13 spheres towards energy minima in phase space were investigated. Our results underline a strong complexity of the hyperdimensional phase space. No simple

rule seems to exist that predicts the final states of spheres starting from different points. Even the global energy minimum appears to exhibit an 'asymmetric' shape. Our results provide evidence of further local energy minima (or shallow saddles) apart from the well-known Σ minima.

Appendix A. Appendix

This appendix provides basic information concerning the mathematics used to calculate the various parameters presented throughout the text. For further information the readers are referred to articles and textbooks devoted to grain boundary geometry (see e.g. [1, 35]) and the paper by Wolf and Lutsko [5] for deeper insight into the idea of Interface Plane Scheme.

Appendix A.1. Misorientation

The (mis-)orientation data output in EBSD is usually given as Euler angles $(\varphi_1, \Phi, \varphi_2)$ (according to Bunge [1, 35]). These can be used to construct the well-known Euler rotation matrix $\mathbf{R}_{Euler}$ for the three dimensional case, not shown here (see e.g. [1, 35]):

This matrix describes the orientation of a sampled part relative to a fixed laboratory coordinate system, i.e. the misorientation between the two coordinate systems. In EBSD, the laboratory coordinate system is rotated into the coordinate system linked to the measured crystal. The misorientation matrix $\Delta\mathbf{R}^{AB}$ between two crystals A and B then arises from the following equation:

$$\Delta\mathbf{R}^{AB} = \mathbf{R}^{A}_{Euler} \cdot (\mathbf{R}^{B}_{Euler})^{-1}. \tag{A.1}$$

The misorientation matrix elements $\Delta\mathbf{R}^{AB}_{ij}$ can then be used to calculate the

misorientation angle and axis $(\Theta_{mis}, \vec{r}_{mis})$ according to:

$$\cos\Theta_{mis} = (\Delta\mathbf{R}^{AB}_{11} + \Delta\mathbf{R}^{AB}_{22} + \Delta\mathbf{R}^{AB}_{33} - 1)/2, \tag{A.2}$$

and

$$
\begin{aligned}
r^1_{mis} &= \Delta\mathbf{R}^{AB}_{32} - \Delta\mathbf{R}^{AB}_{23}, \\
r^2_{mis} &= \Delta\mathbf{R}^{AB}_{13} - \Delta\mathbf{R}^{AB}_{31}, \\
r^3_{mis} &= \Delta\mathbf{R}^{AB}_{21} - \Delta\mathbf{R}^{AB}_{12}.
\end{aligned} \tag{A.3}
$$

It must be noted that depending on the crystallography of the examined system one has to beware of the equivalent solutions resulting from crystal symmetry, i.e. one must account for 24 symmetry operators in the case of cubic systems (see e.g. [34]) which yield 576 equivalent solutions for the misorientaton splitted into 24 misorientation angles, each with one specific rotation axis 24fold permuted in its coordinates. Bearing in mind that misorientation can be related to both grains yields 1152 solutions.

Appendix A.2. Tilt and Twist components

Basically, the Interface Plane Scheme describes the formation of a grain boundary starting from inital single crystalline state as a series of two rotations. First, a rotation about a tilt axis $\vec{r}_{tilt}$ which by definition is perpendicular to the area produced by the two ***future*** grain boundary normals $\vec{n}_1$ and $\vec{n}_2$. A rotation of angle Ψ_{tilt} about $\vec{r}_{tilt}$ leads to the parallel alignment of both grain boundaries normals in an external cordinate system as well as to the formation of the grain boundaries with the two $\vec{n}$ related to the two crystals. A further rotation about one of the grain boundaries normals establishes the twist component ϕ_{twist}. Assuming a grain boundaries orientation (parallel to the substrate surface in our case) and utilizing the Euler orientation matrices for sphere and substrate respectively, the two normals of real grain boundaries can be calculated. The tilt and the twist components can then be determined from the two grain boundary normals according to (for a detailed example of parameter calculations, see [34]):

$$
\begin{aligned}
\sin\Psi_{tilt} &= \left|\vec{n}_1 \times \vec{n}_2\right|, \\
1 + \cos\phi_{twist} &= 2(1 + \cos\Theta_{mis})/(1 + \cos\Psi_{tilt}).
\end{aligned} \tag{A.4}
$$

Acknowledgement

Financial support by the Deutsche Forschungsgemeinschaft (SFB 277: "Grenzflächenbestimmte Materialien") and the Fonds National de la Recherche Luxembourg (AFR: TR-PDR BFR08-16) as well as general support by Dr. Erica T. Lilleodden (Helmholtz-Zentrum Geesthacht) is greatly appreciated.

References

[1] V. Randle, The Measurement of Grain Boundary Geometry (IOP Publishing, Bristol and Philadelphia, 1993).

[2] D. Smith, Interface Sci. **4**, 11 (1996).

[3] D. Wolf, Materials Interfaces: Atomic-Level Structure and Properties, (Chapman and Hall, London, 1992), chap. 1, p. 1.

[4] M. Kronberg and F. Wilson, Trans. AIMME **185**, 501 (1949).

[5] D. Wolf and J. Lutsko, Z. f. Kristallographie **189**, 239 (1989).

[6] W. Read and W. Shockley, Phys. Rev. **78**(3), 275 (1950).

[7] T. Schober and R. Balluffi, Phil. Mag. **21**, 109 (1970).

[8] T. Schober and R. Balluffi, Phil. Mag. **22**, 1063 (1970).

[9] T. Schober and R. Balluffi, Phil. Mag. **24**, 165 (1971).

[10] G. Hasson and C. Goux, Scripta Metall. **5**, 889 (1971).

[11] T. Mori, H. Miura, T. Tokita, J. Haji, and M. Kato, Philos. Mag. Letters **58**, 11 (1988).

[12] H. Miura, M. Kato, and T. Mori, Colloque De Physique C1 **51**, 263 (1990).

[13] G. Palumbo and K. Aust, Materials Interfaces: Atomic-Level Structure and Properties, (Chapman and Hall, London, 1992), chap. 5, p. 190.

[14] U. Wolf, F. Ernst, T. Muschik, M. Finnis, and H. Fischmeister, Phil. Mag. A **66**, 991 (1992).

[15] D. Wolf and K. Merkle, Materials Interfaces: Atomic-Level Structure and Properties, (Chapman and Hall, London, 1992), chap. 3, p. 86.

[16] D. Olmsted, S. Foiles, and E. Holm, Acta Mater. **57**, 3694 (2009).

[17] D. Saylor, A. Morawiec, and G. Rohrer, Acta Mater. **51**, 3663 (2003).

[18] D. Saylor, A. Morawiec, and G. Rohrer, Acta Mater. **51**, 3675 (2003).

[19] G. Rohrer, J. Mater. Sci **46**, 5881 (2011).

[20] C. Hefferan, S. Li, J. Lind, U. Lienert, A. Rollett, P. Wynblatt, and R. Suter, CMC **14**, 209 (2009).

[21] P. Shewmon, Recrystallization, Grain Growth And Textures, (American Society for Metals, Metals Park, Ohio, 1966), chap. 5, p. 165.

[22] G. Herrmann, H. Gleiter, and G. Bäro, Acta metall. **24**, 353 (1976).

[23] R. Maurer, Acta Metall. **35**(10), 2557 (1987).

[24] W. Lojkowski, H. Gleiter, and R. Maurer, Acta Metall. **36**(1), 69 (1988).

[25] U. Erb and H. Gleiter, Scripta Metallurgica **13**, 61 (1979).

[26] H. Kuhn, G. Bäro, and H. Gleiter, Acta Metall. **27**, 959 (1979).

[27] H. Mykura, Acta Metall. **27**, 243 (1979).

[28] S. W. Chan and R. Balluffi, Acta Metall. **33**(6), 1113 (1985).

[29] S. W. Chan and R. Balluffi, Acta Metall. **34**(11), 2191 (1986).

[30] A. Sutton and R. Balluffi, Interfaces in Crystalline Materials, (Oxford Science Publications, 1995), chap. 5, p. 384.

[31] S. W. Chan and V. Boyko, Phys. Rev. B **53**(24), 16579 (1996).

[32] J. Cahn, Ceramic Transactions-Sintering of Advanced Ceramics **7**, 185 (1990).

[33] G. Martin, phys. stat. sol. (b) **172**, 121 (1992).

[34] M. Ziehmer, Untersuchung des Energie-Missorientierung Phasenraums gemischter Cu-Korngrenzen mit Orientierungsabbildender Mikroskopie (OIM) und Kugel-Platte Methode, PhD thesis, Universität des Saarlandes, 66041 Saarbrücken, Germany, 2007.

[35] V. Randle and O. Engler, Introduction to Texture Analysis (Gordon and Breach Science Publishers, Amsterdam, 2000).